MECHANICAL BEHAVIOR OF DLC COATINGS UNDER VARIOUS SCRATCH CONDITIONS

G. Pagnoux[1,2,3], S. Fouvry[1], M. Peigney[2], B. Delattre[3], G. Mermaz-Rollet[3]

[1]LTDS, Ecole Centrale de Lyon, 36 Avenue Guy de Collongue, 69134 Ecully Cedex, France
[2]Laboratoire Navier, Université Paris-Est (Ecole des Ponts ParisTech, IFSTTAR, CNRS),
F-77455 Marne-la-Vallée Cedex 2, France
[3]PSA Peugeot Citroën, Route de Gisy, 78140 Vélizy, France

Abstract: In lubricated sliding contact systems with Diamond-Like Carbon (DLC) coated solids, several studies have shown DLC coatings are highly sensitive to asperities breaking through the lubricant film within the contact area. Those asperities produce damages similar to those obtain from scratch tests, from where coating delamination can initiate and propagate. In the present study, controlled scratches have been performed on DLC-coated samples by varying the tip radius, the normal load and the sliding speed. From one hand, the different fracture mechanisms are compared to those observed on a coated cam-tappet system. They both lead to similar damage and wear, from substrate plasticity to gross spallation, via tensile and angular cracking. On the other hand, a numerical analysis is conducted with a finite element model. It reveals the fracture mechanism can be qualitatively predicted. Additional computations show the scratch severity increases by considering a thinner coating. This upholds the observed experimental coupling between tribochemical wear, scratch networks and coating delamination.

Keywords: DLC; scratch; coating failure; FE model; wear

1   INTRODUCTION

DLC coatings are widely used for their great tribomechanical properties such as their low wear rate and their low coefficient of friction compared to non-coated solutions [1]. Many studies pointed DLC wear mechanisms depend on the atmosphere, on their thickness, their microstructure (hydrogenated or not, doped or not, mono or multi-layered), their interface quality with the substrate and the imposed loading. When applied to an industrial system with complex and various loading, several wear mechanisms can become coupled and a predictive wear model must be seen as a long-term goal.

In lubricated conditions, recent studies highlight the DLC sensibility to particles in the lubricant [2]. In a previous work, the analysis of a cam-tappet system with DLC-coated tappets leads to a complete wear scenario where coating delamination starts around scratch networks and inside tribochemical areas [3]. Scratches may come from particles in the lubricant or asperities on the initial surface of the uncoated counterpart. They are particularly numerous on delaminated tappets, but they do not all lead to delamination. It is then assumed there is a specific scratch severity promoting untimely delamination.

To better understand the link between local scratches and generalized coating failure, simplified tests with controlled scratches need to be conducted. Scratches are performed by a standard scratch tester. Those have been used for many years to assess coating-to-substrate quality, though they do not systematically match the actual scratch conditions. In this study, two DLC coatings have been scratched under various and calibrated conditions and the observed failures are compared to both worn coated tappets and a numerical model.

2   SCRATCH MECHANICS

A scratch test consists in moving at a constant speed a tip on a surface while applying an increasing normal load. Standard scratch tests are performed using a Rockwell C diamond indenter with a 200µm tip radius and a normal load going from 0 to several tenth of Newton. In the case of a coated surface, at a certain critical load the coating will start to fail. The critical loads can be very precisely detected by means of an acoustic sensor attached to the load arm but can also be confirmed and collated with observations from a built-in optical microscope. The critical load data is used to qualify and compare the adhesive or cohesive properties of different film - substrate combinations. In this study, the critical load corresponds to the first observable massive spallation. Multiple failure modes can be observed [4]. It usually starts from substrate

plasticity and a slight residual groove. At a certain point, angular or parallel cracks can be seen at the edge of the groove. Those cracks can also be fully developed beyond the indenter and form conformal or Hertz cracks. With increasing load, a ploughing effect can be seen ahead of the moving tip and several spallation mechanisms appear, from localized chipping to gross spallation. The system response to a scratch test depends on a lot of intrinsic and extrinsic parameters [5]. Holmberg et al. developed a systematic numerical approach to analyze the scratch mechanics, focusing on local stress fields and first crack location [6]. The effect of contact geometry was studied by Xie [7] who pointed out the tip radius highly influences the failure mode.

3   EXPERIMENTAL DETAILS

3.1 Sample description

Samples are circular samples made of AISI M2 steel. They are coated with two different DLC coatings. The first one, named DLC 1, is a hydrogenated multi-layer and doped DLC with an adhesive layer made of chrome. The second one, DLC 2, is a multi-layer coating but non-doped DLC, without adhesive layer. They are similar to those used in the cam-tappet system evoked previously. Both substrate and coating were characterized by nanoindentation and EDX analysis. The coating structure and thickness and the different material parameters are listed in table 1 (where data with "*" means values which were not measured).

Table 1 - Material properties

	Substrate	DLC 1	DLC2
Structure	AISI M2	Cr+CrN+a-C:H:Si+a-C:H	WC+WCC+a-C:H
Thickness [mm]	5	$0.9e^{-3}$ (Cr+ CrN) + $2.5e^{-3}$ (a-C:H :Si + a-C:H)	$0.9e^{-3}$ (WC+ WCC) + $2.5e^{-3}$ (a-C:H)
Hardness	62 [HRC]	3600 [HV]	3900 [HV]
Ra [µm]	0.02	0.21	0.15
E [GPa]	210*	223	239
v	0.27*	0.2*	0.2*
Yield limit [MPa]	4500*		

3.2 Scratch tests

Scratches have been performed using a CSM scratch tester and a Rockwell C diamond indenter with a spherical tip and a 120° cone angle. In a previous work, a simplified numerical model has been created to estimate the load transmitted by asperities [8]. As a result, a scratch map has been defined to represent the contact conditions of a coated cam-tappet system from an automotive engine which encounters asperities. The tip radius (10, 20, 50, 100 and 200µm) and scratch length (1 to 5mm) have been chosen to cover the range of observed ones on cam-tappet systems, while the normal load is raised until failure or until the maximum load given by the scratch map. The tip speed has been set to 1 and 100mm/min. Before tests, the specimens where cleaned with acetone.

4   OBSERVATIONS

In the following section, the main results from DLC 1 tests will be highlighted. For 10µm and 20µm tip radius tests, either nothing or only a slight residual groove coming from substrate plasticity is observed. This means the main stress field generated (up to a maximal contact pressure of 20GPa) is restricted to the coating and do not exceed the yield limit of the substrate, so a quasi-full elastic recovery arises after the tip transit. With the 50µm tip radius tests come the first observable cracks, which can be classified as tensile to Hertz cracks (fig. 1). However, at the maximum imposed normal load, no critical failure can be observed.

There are multiple mechanisms of failure with 100µm tip radius tests (fig. 2). The coating exhibits substrate plasticity between 0 and 2.5N. Surface angular cracks located at the groove edge start to appear at 2.5N and become more numerous up to 5.8N. They also become longer by propagating toward the groove center with a slight curvature. At 5.8N, the first critical failure is observed with the creation of large circular spalls alternatively located from one side of the wear track to another. The entire coating is removed as the remaining material is the substrate. Spalling occurs until the end of the scratch.

200µm scratch tests (fig. 3) are quite similar to 100µm ones. Angular cracks appear at 12.1N and propagate to the groove center with a slight curvature at low load, then straight to the center with higher ones. Chipping occurs at 17.8N, followed closely by critical failures from 18.2N to the end of the scratch. The spalls from 200µm tests seem to have a thinner profile than those of 100µm, but a comparative analysis indicates all spalls have actually the same average dimensions.

There is no major difference between scratches at 1 and 100mm/min, meaning there is no viscous effect acting at such speed. Despite the sliding speeds are widely inferior to those acting in the actual cam-tappet systems (up to several m/s), the present scratches exhibit similar failure mode, although spalling is rarely observed on coated tappets. This is relevant with the scratch map, in which most of the calculated load transmitted by asperities does not exceed the observed critical load.

The same scratches have been performed on samples coated with DLC 2. While both DLC are hydrogenated DLC and have the same thickness, they behave differently. DLC 2 exhibits similar failure modes but with higher critical loads. Thus, DLC 2 has a better fracture resistance, although it does not have an adhesive layer. This confirms the high dependence of the coating mechanical behavior to its intermediate layers.
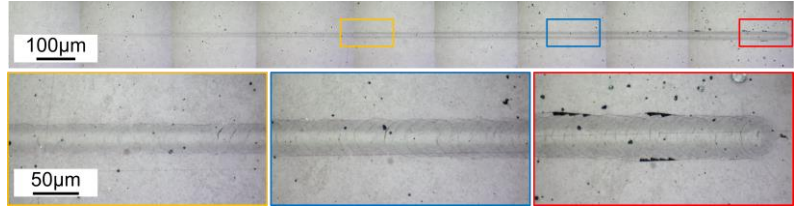

Figure 1 - R = 50µm, Fn = 0.03 – 2.0N, L = 2mm, v = 1mm/min
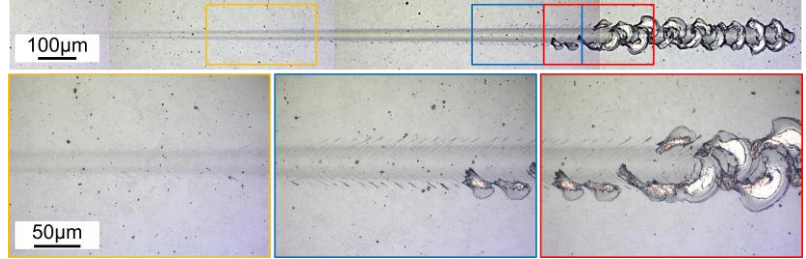
Figure 2 - R = 100µm, Fn = 0.03 – 7.5N, L = 2mm, v = 1mm/min
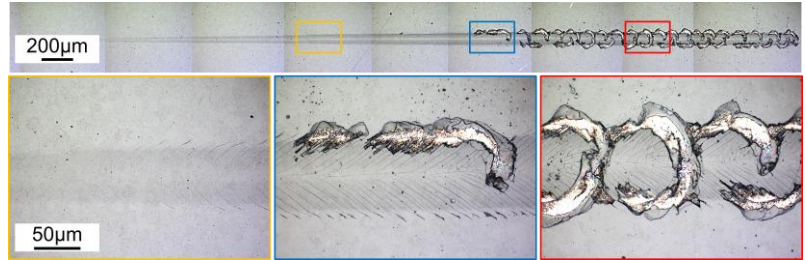
Figure 3 - R = 200µm, Fn = 0.03 – 23.5N, L = 5mm, v = 1mm/min

Indeed, they do not only reduce the intrinsic coating residual stress. Crack fronts propagate differently from one layer to another, meaning it would be necessary to identify the associated fracture toughness of each constitutive layer to correctly catch the full coating fracture behavior. By extrapolation, this knowledge would be of great matter to estimate the coating behavior under complex loadings, such as those experienced in cam-tappet systems. Unfortunately, the thickness of DLC coatings makes it difficult if not impossible to obtain.
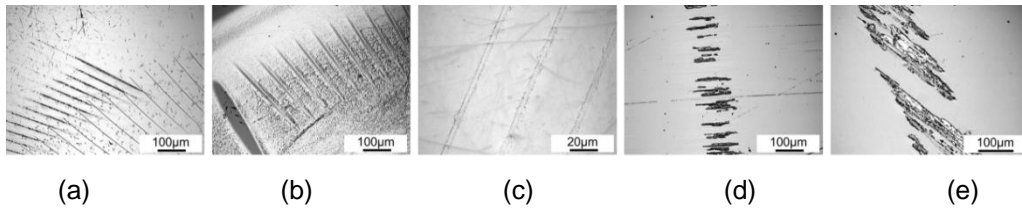

(a) (b) (c) (d) (e)

Figure 4 - Scratch network examples from a cam-tappet system [3]

5   NUMERICAL ANALYSIS AND DISCUSSION

In this numerical analysis, we focus on one substrate, one coating (DLC 1) and several scratch conditions. The substrate is chosen elastic perfectly plastic, without hardening. The coating is assumed homogeneous, isotropic and fully elastic. The surface and interface are perfectly smooth and the indenter is chosen has a perfectly rigid sphere. No residual stress is taken into account, as they were not measured on the scratched samples. The material parameters are taken from table 1, and the coefficient of friction has been set to 0.15, according to the average data measured during tests. The boundaries are at least 5 to 10 times away from the contact area. Due to theoretical symmetry from both side of the scratch track, only half of the geometry was modeled. There is a minimum of 10 elements in the contact half-length and at least 7 elements in the coating thickness. All elements are three-dimensional tetrahedral elements, for a total of around $2e^5$ elements (fig. 5).

The loading is chosen as a 3 phase loading. The tip is firstly put into contact with the surface then a constant normal force is imposed as well as a longitudinal displacement. The last step consists in removing the indenter by applying an imposed normal and longitudinal displacement. The scratch length is chosen so that a steady state is reach at the end of the loading step. The full scratch test is not represented as it would require too many elements. As a result, the model can only be representative of an instant of the scratch test. The numerical model has been run for every scratch configuration. The chosen constant load was either the identified critical load or the maximal load, depending on whether or not a critical failure has been observed during scratch.
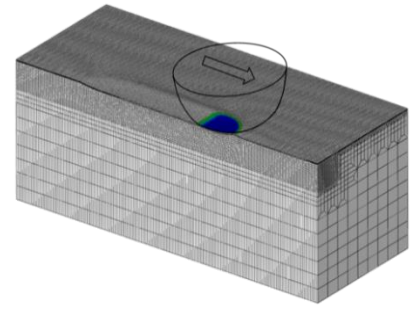

Figure 5 - Illustration of the FE model

The first result to highlight is the correlation between the observed cracks before critical failure (dashed line on figure 6 (a-c), top) and the direction perpendicular to the direction of the maximal principal stress on the surface (figure 6 (a-c), bottom). This means, as expected, the coating behaves as a brittle material and the first crack initiates on the surface, driven by the principal stress directions, and propagates toward the interface. Those results are similar to the mechanism of crack initiation developed in [6]. It can also be pointed out that the maximum stress value from which angular cracks start to appear are similar from one test to the other, and equals approximately XXX MPa at 0.8, 2.5 and 12N, respectively.

(a) R = 50µm, at 2.0N   (b) R = 100µm, at 5.8N   (c) R = 200µm, at 18.2N
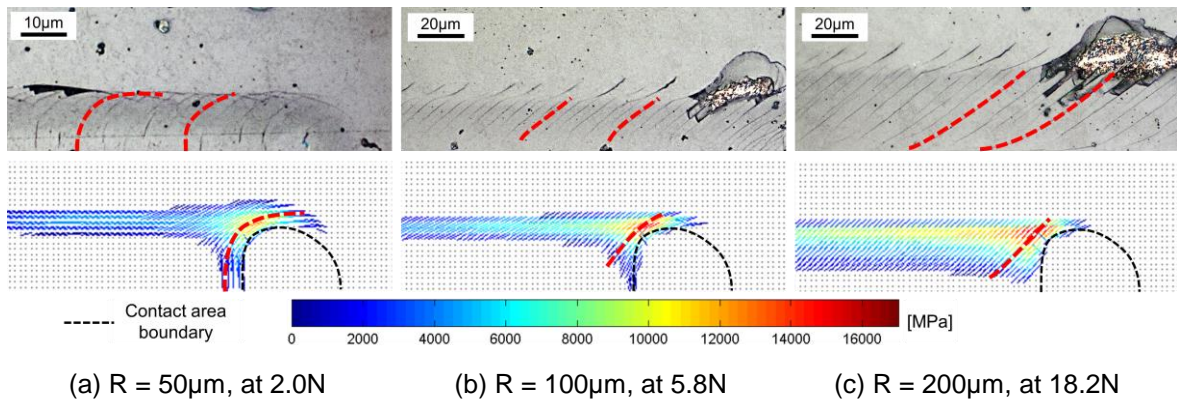
Figure 6 – Surface cracks before failure (top) and first principal stress at the critical load (bottom)

The critical failure is characterized here by massive spall creation up to the interface. This means the system dissipates the stored energy accumulated in the coating by cracking in the surface as well as in the interface, via through thickness cracking. At the interface for instance, failure can be due to an excess of shear or normal traction. Another common loading mode is the excess of compressive stress ahead of the indenter that causes buckling of the coating. Each mechanism tends to dissipate energy so, as a global approach, one can analyses the recoverable energy density in the coating, at its surface and in the interface. However, the entire recoverable energy does not contribute to crack initiation and propagation. By assuming a virtual surface crack front initiated perpendicularly to the direction of the maximal principal stress ($\underline{n}_s$, fig. 7), the surface energy density required for it to propagate can be seen as part of the total available energy density.
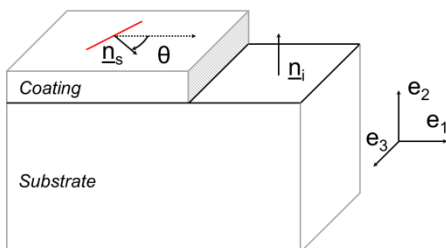

Figure 7 - Virtual surface crack and normal vector illustration

It can be expressed as in eq. (1), where $\underline{n}_s$ refers to the projection of the direction of the maximal principal stress on the surface and $\underline{\underline{\sigma}}^*$ equals $\underline{\underline{\sigma}}$, except $\sigma_{ii}^* = \max(0, \sigma_{ii})$.

This means compressive stresses are not included in the calculated energy density, as they do not contribute to initiate nor propagate the considered virtual crack.

$$w_s = \frac{1}{2}\left(\underline{n}_s \cdot \underline{\underline{\sigma}}^* \cdot \underline{\underline{\varepsilon}} \cdot \underline{n}_s \right). \tag{1}$$

At the interface and based on the work of Pradeilles-Duval [9], the calculated energy density corresponds to the jump of energy density across the interface minus the normal part of it, as it is the only part which does not participate in any mode of failure. The energy is expressed as in eq. (2), where $\underline{n}_i$ refers to the normal at the interface (fig. 7), $|[\ ]|$ to the jump of value across the interface, $< >$ to the mean value at the interface, and w is the total energy density.

$$w_i = |[w]| - \frac{1}{2} < \underline{n}_i \cdot \underline{\underline{\sigma}} > . \left| \left[\underline{\underline{\varepsilon}} . \underline{n}_i \right] \right|. \tag{2}$$

The stress state complexity before critical failure implies the used numerical model cannot be as representative of the system as it is at lower loads, especially considering it does not take into account the energy released by previous existing cracks. However, there is an acceptable correlation between the calculated energy densities and the failure modes. On surface, for 50µm scratch test, the recoverable energy concentrates at the indenter side and is split in two behind it (fig. 8 (a), top). One part remains in the groove edge due to substrate plasticity and coating residual strain while the other follows the tip back. Since there is no noticeable ploughing, the energy at the interface is almost homogeneously located under the indenter (fig. 8 (a), bottom). As a result, there are few risks of developing spalls in this circumstance and only tensile nay Hertz cracks may appear.
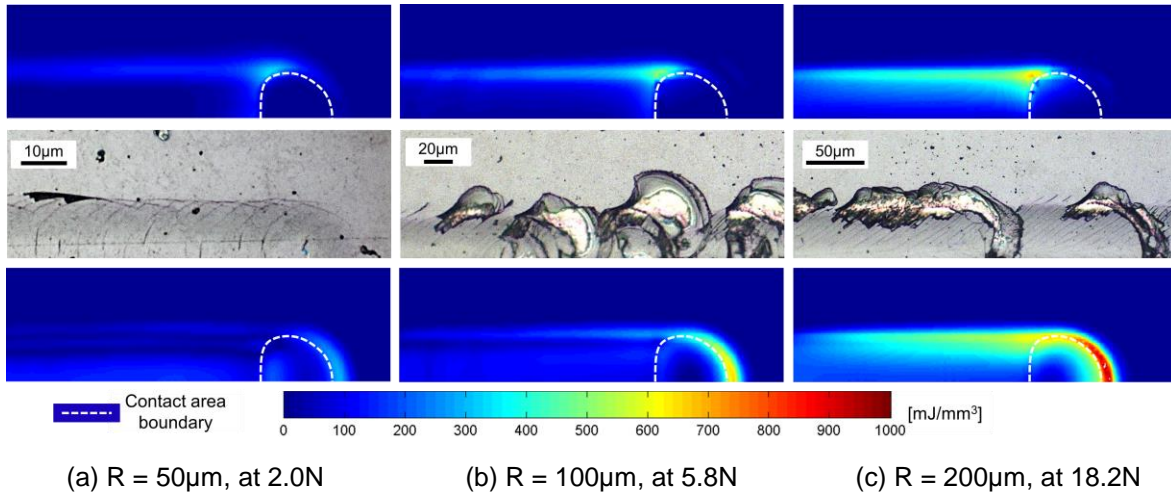

(a) R = 50µm, at 2.0N   (b) R = 100µm, at 5.8N   (c) R = 200µm, at 18.2N

Figure 8 – Surface (w_s, top) and interface (w_i, bottom) energy density

For 100µm and 200µm scratch tests, the energy levels dramatically increase as a result of a significant ploughing effect. At the surface, the higher values of the energy density extend from the side to the back-side of the contact area (fig. 8 (b-c), top). At the interface, the recoverable energy concentrates in the tip front, mainly due to the compression of the coating in the sliding direction (fig. 8 (b-c), bottom). For 200µm tests, there is a massive overlap between the area of maximal energy density at the surface and at the interface. Thus, the following failure's kinetics is proposed: first cracks are developed on surface, behind the tip and at the groove edge and propagate toward the interface. This propagation depends on the direction of the maximal principal stress. Cracks are likely to bifurcate toward the area of highest energy density, facilitated by the overlap between areas of maximal energy density. Consequently, they turn into the initial defects required for the coating to buckle, due to excessive compression at the front-side and front of the tip. This kinetics is consistent with the nano-scratch failure behavior proposed in [11]. Furthermore, it has been shown a bigger tip radius leads to an increase of the compressive stress and a decrease of the bending one [7]. This effect, combined with the decrease of the critical buckling stress with the radius of the loaded region [10], drastically enhances the probability of coating spallation.

The numerical model was also used to simulate the same scratch conditions but with a partially worn coating (i.e. with a reduced thickness). Results shown higher stress levels (and energy density) for the worn coatings. This upholds the scratch severity increases with wear, and that scratches made by asperities after a long-term test may be more severe than those realized during a running-in period. After the indenter removal, the recoverable energy stored in the coating is of the same order than the one existing during scratch, particularly at the groove edge. Therefore, in the cam-tappet system, the initial scratches created

by asperities are more likely going to evolve into generalized coating delamination when coupled with tribochemical wear.

6   CONCLUSION

Two different hydrogenated DLC coatings have been scratched under various conditions by varying the tip radius, the normal load and the sliding speed. The wear mechanisms include substrate plasticity, cracks and spallation. The more severe scratches are those with the bigger tip radius. This is due to the ploughing effect arising at bigger loads, which promote compressive stress and buckling-like failure mode ahead of the indenter. Observations demonstrate the mechanical behavior of each constitutive layer of the coating has to be evaluated to correctly catch the actual coating behavior under fracture. Before critical failure, the numerical model confirms the coating behaves as a brittle material and first cracks appears at the surface, behind the contact area and at the groove edge, driven by the maximal principal stress. The analysis of the maximal energy density areas at the surface and at the interface allows suggesting a failure's kinematics explaining the origin of the initial defect required for the coating to buckle. The numerical model also highlights that for a given scratch, a worn (i.e. thinner) coating is more sensitive than an unworn one by storing a higher recoverable energy after the indenter removal. This is in agreement with observations on complex environments like coated cam-tappet systems, where generalized delamination initiates around scratch networks and inside tribochemically worn area.

7   ACKNOWLEDGEMENTS

8   REFERENCES

[1] C. Donnet, A. Erdemir, Tribology of diamond-like carbon films: Fundamentals and applications, Springer, 2008.

[2] T. Haque, D. Ertas, et al., The role of abrasive particle size on the wear of diamond-like carbon coatings, Wear, 302(1-2), 882-889, 2013.

[3] G. Pagnoux, S. Fouvry, et al, Usures et endommagements des revêtements DLC sur systèmes came-poussoir, Tribologie: Fondamentaux et Applications Complexes, 1-8, 2013.

[4] S. Bull, Failure modes in scratch adhesion testing, Surface and Coatings Technology, 50(1), 25-32, 1991.

[5] S. Bull, E. Berasetegui, An overview of the potential of quantitative coating adhesion measurement by scratch testing, Tribology International, 39(2), 99-114, 2006.

[6] K. Holmberg, A. Laukkanen, et al., Tribological analysis of fracture conditions in thin surface coatings by 3D FEM modelling and stress simulations, Tribology International, 38 (11-12), 1035-1049, 2006.

[7] Y. Xie, H. M. Hawthorne, Effect of contact geometry on the failure modes of thin coatings in the scratch adhesion test, Surface and Coatings Technology, 155(2), 121-129, 2002.

[8] G. Pagnoux, S. Fouvry, et al, A model for single asperity perturbation on lubricated sliding contacts with DLC-coated solids, 40th Leeds-Lyon Symposium on Tribology and Tribochemistry Forum, Lyon, France, 2013.

[9] R. M. Pradeilles-Duval, C. Stolz, Mechanical transformations and discontinuities along a moving surface, Journal of the Mechanics and Physics of Solids, 43(1), 91-121, 1995.

[10] H. E. Evans, Modelling oxide spallation, Materials at high temperatures, 12(2-3), 219-227, 1994.

[11] L. Huang, J. Lu, et al, Elasto-plastic deformation and fracture mechanism of a diamond-like carbon film deposited on a Ti–6Al–4V substrate in nano-scratch test, Thin Solid Films, 466(1), 175-182, 2004.